Table 2: GISMO (150 GHz) fluxes of the observed clusters.

Cluster	Obs. Date	RA	DEC	Tau	Exposure (min)	CRUSH Option	Flux (mJy)	FWHM (“)	Peak (mJy)	Map RMS
Epoch 1 : April 2012										
Z235	20/04/12	00:43:52.30	24:24:24.5	0.32	10	-faint	4.7 ± 1.2	18.0	4.4	0.9
RXJ0132-08	20/04/12	01:32:41.16	-08:04:07.6	0.17	7	-faint	28.8 ± 4.7	17.7	30.9	1.1
MACS0242-21	21/04/12	02:42:36.11	-21:32:27.3	0.20	2	-faint	35.6 ± 6.0	18.1	37.5	1.8
A496	21/04/12	04:33:37.82	-13:15:46.5	0.23	10	-faint	6.1 ± 1.3	16.4	5.9	0.9
RXJ0439+05	18/04/12	04:39:02.32	05:20:37.0	0.35	5	-faint	56.0 ± 9.2	16.4	56.5	2.1
PKS0745-191	18/04/12	07:47:31.34	-19:17:42.7	0.19	25	-faint	4.9 ± 1.1	21.9	4.7	0.8
A646	17/04/12	08:22:08.86	47:05:54.1	0.49	20	-faint	11.5 ± 2.1	13.4	10.9	1.0
4C+55.16	17/04/12	08:34:55.21	55:34:20.6	0.10	2	-faint	81.7 ± 13.2	15.6	79.4	1.7
Hydra-A	17/04/12	09:18:05.84	-12:05:41.1	0.14	4	-faint	266.7 ± 42.7[7]	24.8	179.9	2.3
A1348	18/04/12	11:41:24.26	-12:16:37.7	0.15	2	-faint	<6.3	-	-	2.1
RXJ1347-11	21/04/12	13:47:31.84	-11:45:10.9	0.20	20	-deep	<3.3	-	-	1.1
RXJ1350+09	11/04/12	13:50:22.01	09:40:16.9	0.10	10	-faint	16.0 ± 2.8	12.7	14.9	1.1
A3581	21/04/12	14:07:30.19	-27:01:08.6	0.18	2	-faint	71.0 ± 11.6	16.4	72.4	2.1
AS780	18/04/12	14:59:29.98	-18:10:47.8	0.10	5	-faint	17.0 ± 3.2	16.1	16.0	1.6
A2052	11/04/12	15:16:44.50	07:01:16.8	0.10	30	-faint	41.7 ± 6.7	17.3	42.5	0.7
A2055	22/04/12	15:18:46.13	06:13:49.3	0.26	5	-faint	13.2 ± 2.5	17.2	12.9	1.3
RXJ1558-14	18/04/12	15:58:22.19	-14:10:02.7	0.10	5	-faint	39.2 ± 6.4	14.4	38.4	1.5
Z8193	18/04/12	17:17:19.06	42:26:59.2	0.13	2	-faint	12.8 ± 3.1	10.5	13.8	2.7
A2270	18/04/12	17:27:23.71	55:10:52.3	0.11	2	-faint	70.8 ± 4.1	14.9	70.0	2.4
Z8276	23/04/12	17:44:14.88	32:59:30.8	0.29	5	-faint	35.1 ± 5.8	17.4	36.8	1.3
E1821+644	18/04/12	18:21:57.49	64:20:35.6	0.13	10	-faint	5.8 ± 2.8	13.3	5.4	1.4
RXJ1832+68	18/04/12	18:32:35.80	68:48:06.3	0.12	10	-faint	10.0 ± 2.3	11.5	9.3	1.7
MACS1931-26	21/04/12	19:31:49.74	-26:34:33.2	0.12	20	-faint	7.2 ± 2.1	18.9	7.6	0.9
A2390	22/04/12	21:53:36.74	17:41:40.2	0.09	10	-faint	8.1 ± 1.6	13.3	7.7	0.9
A2415	18/04/12	22:05:38.62	-05:35:35.1	0.12	5	-faint	31.2 ± 5.3	19.1	33.0	1.9
A2597	18/04/12	23:25:19.93	-12:07:26.8	0.11	5	-faint	15.0 ± 2.8	16.3	15.2	1.4
A2627	20/04/12	23:36:42.29	23:55:31.4	0.40	5	-faint	16.8 ± 3.0	17.9	16.8	1.3
RXJ2341+00	18/04/12	23:41:07.10	00:18:30.9	0.10	5	-faint	41.8 ± 6.9	16.1	42.2	1.5
Epoch 2 : November 2012										
RXJ0352+19	31/10/12	03:52:58.97	19:40:59.6	0.13	10	-deep	<3.6	-	-	1.2
RXJ0439+05	31/10/12	04:39:02.11	05:20:42.9	0.15	5	-faint	52.0 ± 8.5	16.6	52.5	1.6
PKS0745-191	31/10/12	07:47:31.30	-19:17:45.9	0.13	5	-faint	5.8 ± 1.8	17.8	5.3	1.5
A646	31/10/12	08:22:10.05	47:05:54.9	0.10	6	-faint	11.4 ± 2.1	18.4	12.0	1.0
4C+55.16	31/10/12	08:34:55.26	55:34:22.9	0.13	5	-faint	77.8 ± 12.5	18.0	80.1	1.4
Hydra-A	31/10/12	09:18:05.83	-12:05:46.5	0.11	5	-faint	273.8 ± 43.8[7]	24.5	167.8	1.8
A1084	31/10/12	10:44:33.11	-07:04:11.1	0.11	10	-faint	4.5 ± 1.2	19.0	4.1	1.0
A1348	31/10/12	11:41:24.37	-12:16:40.0	0.11	5	-faint	6.9 ± 1.7	10.7	6.5	1.3
A1774	31/10/12	13:41:05.19	39:59:47.1	0.15	10	-faint	6.9 ± 1.5	19.7	6.9	1.0
RXJ1347-11	31/10/12	13:47:31.84	-11:45:10.9	0.12	10	-deep	<3.0	-	-	1.0
A1795	31/10/12	13:48:52.25	26:35:32.2	0.19	10	-faint	5.1 ± 1.4	17.7	5.4	1.1
RXJ1350+09	31/10/12	13:50:22.04	09:40:07.9	0.19	10	-faint	16.0 ± 2.7	17.0	15.7	1.0
A3581	31/10/12	14:07:30.00	-27:01:07.8	0.12	5	-faint	62.1 ± 10.1	19.0	63.2	2.0
A1885	31/10/12	14:13:43.86	43:39:40.0	0.10	10	-deep	4.0 ± 1.0	12.4	4.2	0.8
AS780	31/10/12	14:59:29.14	-18:10:51.3	0.11	10	-faint	15.4 ± 2.7	17.9	15.3	1.2
A2052	31/10/12	15:16:44.64	07:01:16.3	0.11	5	-faint	38.0 ± 6.3	16.3	38.4	1.7
A2055	02/11/12	15:18:46.19	06:13:56.5	0.50	10	-faint	10.4 ± 2.5	18.9	10.2	1.8
RXJ1558-14	31/10/12	15:58:22.22	-14:10:03.1	0.11	5	-faint	27.8 ± 4.8	15.1	27.6	1.9
NGC6338	31/10/12	17:15:23.25	57:24:41.5	0.12	10	-faint	7.3 ± 1.5	11.0	6.8	1.0
Z8193	31/10/12	17:17:19.11	42:26:59.2	0.11	10	-faint	15.6 ± 2.8	15.9	15.0	1.2
A2270	31/10/12	17:27:23.52	55:10:52.5	0.11	5	-faint	56.2 ± 9.1	18.0	58.3	1.3
Z8276	02/11/12	17:44:14.82	32:59:27.4	0.53	10	-faint	12.5 ± 2.7	16.1	13.2	1.8
E1821+644	31/10/12	18:21:57.00	64:20:32.9	0.11	10	-faint	7.9 ± 1.7	11.3	7.8	1.2

[7] Resolved source, integrated flux

Table 2 – Continued

Cluster	Obs. Date	RA	DEC	Tau	Exposure (min)	CRUSH Option	Flux (mJy)	FWHM (“)	Peak (mJy)	Map RMS
RXJ1832+68	31/10/12	18:32:35.08	68:48:02.2	0.12	7	-faint	8.9 ± 1.7	17.2	9.0	1.0
Epoch 3 : April 2013										
RXJ0132-08	11/04/13	01:32:41.05	-08:04:07.8	0.83	5	-faint	27.6 ± 13.7	17.4	24.0	13.0
M0242-21	11/04/13	02:42:35.99	-21:32:24.9	0.70	10	default	17.9 ± 6.6	15.4	22.9	6.0
A496	10/04/13	04:33:37.75	-13:15:40.7	0.57	20	-faint	4.4 ± 1.1	13.1	4.3	0.8
RXJ0439+05	10/04/13	04:39:02.31	05:20:42.7	0.69	5	-faint	47.6 ± 7.8	17.4	48.6	1.6
A646	10/04/13	08:22:09.50	47:05:53.4	0.59	10	-faint	12.2 ± 2.3	10.7	11.4	1.3
4C+55.16	10/04/13	08:34:54.79	55:34:19.8	0.63	5	-faint	61.7 ± 10.0	16.9	62.7	1.8
Hydra-A	10/04/13	09:18:05.79	-12:05:39.6	0.61	5	-extended	201.9 ± 32.9[7]	25.0	153.5	6.2
RXJ1504-02	11/04/13	15:04:07.43	-02:48:15.8	0.59	10	-faint	5.5 ± 1.4	11.2	5.1	1.1
A2052	11/04/13	15:16:44.48	07:01:18.9	0.58	5	-faint	35.0 ± 5.8	17.0	36.6	1.6
RXJ1558-14	11/04/13	15:58:22.01	-14:09:58.2	0.63	5	-faint	25.1 ± 4.3	14.9	23.8	1.6
A2270	11/04/13	17:27:23.58	55:10:52.8	0.64	5	-faint	50.4 ± 8.2	14.5	51.2	1.7
Z8276	11/04/13	17:44:14.47	32:59:29.4	0.68	5	default	<44.7	-	-	14.9
A2390	11/04/13	21:53:36.96	17:41:40.4	0.65	10	-faint	8.6 ± 2.0	14.1	8.6	1.4
A2415	11/04/13	22:05:38.64	-05:35:31.7	0.65	5	-faint	26.7 ± 4.7	16.3	25.8	1.9
A2627	11/04/13	23:36:41.84	23:55:28.2	0.66	10	-faint	16.9 ± 3.0	14.9	15.9	1.3
RXJ2341+00	15/04/13	23:41:07.01	00:18:33.0	0.39	5	-faint	33.0 ± 2.9	15.2	32.5	1.8

Table 3: AMI (16 GHz) fluxes of the observed BCGs.

Cluster	Obs. Date	Flux	RMS	Obs. Date	Flux	RMS	Obs. Date	Flux	RMS
Z235	11/04/12	17.7 ± 0.9	0.2	04/06/12	16.7 ± 0.9	0.3	-	-	-
RXJ0132-08	17/04/12	139.5 ± 8.3	4.5	02/06/12	126.1 ± 6.9	2.7	-	-	-
RXJ0439+05	12/04/12	324.8 ± 16.3	1.6	30/05/12	307.5 ± 15.5	2.1	29/09/12	299.9 ± 15.1	2.0
A646	10/04/12	45.6 ± 2.3	0.5	30/05/12	45.7 ± 2.7	1.4	27/09/12	47.3 ± 2.5	0.7
4C+55.16	14/04/12	1317.7 ± 66.0	3.5	30/05/12	1372.3 ± 70.6	16.8	-	-	-
RXJ1350+09	24/04/12	133.7 ± 6.7	0.9	14/06/12	107.4 ± 5.6	1.5	-	-	-
A2052	24/04/12	231.8 ± 11.8	2.2	14/06/12	220.8 ± 11.2	1.9	-	-	-
A2055	24/04/12	66.7 ± 3.5	1.2	14/06/12	68.6 ± 3.6	1.2	-	-	-
Z8193	24/04/12	79.8 ± 4.1	1.1	26/06/12	79.3 ± 4.1	1.2	-	-	-
A2270	24/04/12	185.0 ± 9.4	1.6	26/06/12	253.8 ± 12.8	1.4	26/09/12	226.9 ± 11.6	2.6
Z8276	14/04/12	88.6 ± 4.5	0.7	31/05/12	95.9 ± 4.9	0.8	26/09/12	87.6 ± 4.6	1.3
E1821+644	25/04/12	9.0 ± 0.5	0.2	30/06/12	10.8 ± 0.8	0.2	-	-	-
RXJ1832+68	19/05/11	45.6 ± 2.3	0.4	25/04/12	42.2 ± 2.1	0.1	05/07/12	42.3 ± 2.1	0.3
A2390	14/04/12	68.5 ± 12.4	0.8	31/05/12	66.4 ± 3.4	0.9	-	-	-
A2415	11/04/12	77.4 ± 4.2	1.7	02/06/12	77.2 ± 4.5	2.3	-	-	-
A2627	14/04/12	83.1 ± 4.2	0.7	31/05/12	73.3 ± 4.0	1.5	-	-	-
RXJ2341+00	11/04/12	147.0 ± 7.4	1.2	31/05/12	140.9 ± 7.2	1.5	28/09/12	209.2 ± 11.8	5.4

Table 4: CARMA (90 GHz) fluxes of the observed BCGs.

Cluster	Obs. Date	RA	DEC	Flux	RMS
Z235	11/06/12	00:43:52.21	24:24:21.5	9.9 ± 1.8	4.5
RXJ0132-08	21/05/12	01:32:41.11	-08:04:05.7	98.8 ± 11.9	6.7
MACS0429-02	15/06/12	04:29:36.00	-02:53:07.0	<14.1	4.7
A496	15/06/12	04:33:37.89	-13:15:42.3	11.4 ± 3.6	3.4
RXJ1350+09	21/05/12	13:50:22.12	09:40:10.7	22.8 ± 2.8	1.7
A3581	21/05/12	14:07:29.83	-27:01:04.2	82.5 ± 9.1	2.8
AS780	21/05/12	14:59:28.78	-18:10:44.9	29.5 ± 4.4	2.3
A2052	21/05/12	15:16:44.58	07:01:18.1	126.7 ± 14.3	9.1
A2055	21/05/12	15:18:46.45	06:13:57.9	53.6 ± 9.0	21.6
RXJ1504-02	21/05/12	15:04:07.50	-02:48:16.9	8.3 ± 1.6	1.4
RXJ1558-14	21/05/12	15:58:21.91	-14:09:58.9	44.8 ± 4.9	6.3
Z8193	22/05/12	17:17:19.21	42:26:57.8	22.4 ± 2.9	1.8
A2270	22/05/12	17:27:23.49	55:10:53.9	164.7 ± 17.2	14.4
Z8276	22/05/12	17:44:14.47	32:59:27.4	35.4 ± 6.0	4.9
E1821+644	24/05/12	18:21:56.24	64:20:58.0	7.2 ± 1.8	1.7
RXJ1832+68	22/05/12	18:32:35.52	68:48:07.2	19.6 ± 4.0	3.5
MACS1931-26	11/06/12	19:31:49.64	-26:34:32.4	9.6 ± 2.9	2.7
A2390	04/06/12	21:53:36.81	17:41:44.8	22.3 ± 3.2	2.3
A2415	04/06/12	22:05:38.53	-05:35:33.7	25.7 ± 3.4	2.3
A2597	21/05/12	23:25:19.82	-12:07:28.6	19.7 ± 5.8	2.0
A2627	04/06/12	23:36:42.82	23:55:23.8	19.8 ± 4.5	4.0
RXJ2341+00	21/05/12	23:41:06.94	00:18:33.3	72.8 ± 8.0	3.2

Table 5: SCUBA-2 (353 GHz) fluxes of the observed BCGs.

Cluster	Obs. Date	Flux (mJy)	RMS
RXJ0132-08	23/10/12	-	13.1
MACS0242-21	01/10/12	34.0	7.6
RXJ0439+05	01/10/12	18.7	5.2
A646	27/02/12	25.9	6.6
4C+55.16	27/02/12	29.0	6.5
Hydra-A	08/10/12	76.3	8.8
A1348	27/12/12	-	7.9
RXJ1347-11	29/12/12	-	5.5
A1795	27/12/12	-	7.4
RXJ1350+09	23/02/12	-	5.7
A3581	28/01/13	59.2	9.1
AS780	15/04/12	-	5.0
RXJ1504-02	12/01/13	13.7	4.0
A2052	28/01/13	-	7.8
RXJ1558-14	15/04/12	40.3	4.7
Z8193	14/05/12	-	8.5
A2270	30/09/12	34.9	4.7
Z8276	30/09/12	27.7	5.0
RXJ1832+68	05/09/12	-	5.8
MACS1931-26	16/09/12	16.8	4.8
A2390	24/04/13	-	4.9
A2415	01/10/12	18.2	6.7
A2597	24/10/12	-	7.2
A2627	24/10/12	20.1	7.3
RXJ2341+00	31/08/12	33.2	3.9

APPENDIX A: NOTES ON INDIVIDUAL SOURCES

Individual source SEDs were populated using the main radio catalogues (e.g. Australia Telescope 20 GHz Survey (AT20G), Murphy *et al.* 2010; NVSS and Faint Images of the Radio Sky at Twenty-cm (FIRST) at 1.4 GHz, Condon *et al.* 1998; White *et al.* 1997; SUMSS at 843 MHz, Mauch *et al.* 2003; Texas Survey of Radio Sources (TEXAS) at 365 MHz, Douglas *et al.* 1996; Westerbork Northern Sky Survey (WENSS) and Westerbork In the Southern Hemisphere (WISH) at 325 MHz, Rengelink *et al.* 1997; De Breuck *et al.* 2002; VLA Low-Frequency Sky Survey (VLSS) at 74 MHz, Cohen *et al.* 2007), the NASA/IPAC Extragalactic Database (NED) and the High Energy Astrophysics Science Archive Research Center (HEASARC) database, the National Radio Astronomy Archive (NRAO), literature searches, the data presented herein and supplemented by data from H15a.

Due to the lack of self-similarity between these spectra each source was fit on an individual basis. Where possible, active components were isolated and fit using the GPS model of (Orienti & Dallacasa 2014, :)

$$Log(S) = A_0 + Log(\nu)(A_1 + A_2 Log(\nu)) \quad \text{(A1)}$$

Steep spectrum components and active flat spectrum components where no peak was apparent were both fit using a simple power-law of the form:

$$\mathbf{S} = \mathbf{A}\nu^{-\alpha} \quad \text{(A2)}$$

Where both an active and inactive component were found to be present, the core contribution is removed from the total emission prior to fitting the more extended emission. In a couple of cases clear spectral curvature attributable to synchrotron ageing is present in the steeper spectrum components and is modelled as described in the notes below. Additionally, flattening of a steep spectrum component to low frequencies (below 100MHz) is seen in a minority of sources. Where morphologically it is clear that this is extended emission, and hence **the flattening is** most likely due to free-free absorption then these data are excised from the fits as described below.

4C+55.16
2MFGC 06756, z=0.2411. This is a powerful radio source that is clearly extended on milliarcsecond scales as observed using VLBI (Helmboldt 2007, see also Hogan *et al.* 2015c, in prep.). The SED has a flat index in the GHz range that appears to be caused by the superposition of a broad peaked GPS-like component with a steep spectrum power-law component to lower frequency (below about 100 MHz). The SED is fit using a GPS-like model with parameters **A_0=3.90±0.03, A_1=-0.04±0.02 and A_2=-0.43±0.01** and a steep power-law to lower frequency with α=1.1±0.1 and A=500.0±10.0.
A1084
2MASX J10443287-0704074, z=0.1326. The SED is sparsely sampled, although the non-detection in VLSS (Cohen *et al.* 2007) coupled to its flat returned index shows the source to be core-dominated. The SED is fit with a power-law of α=0.36±0.04 and A=36.7±2.9.
A1348
LCRS B113851.7-115959, z= 0.1195. The source is best fit using a GPS-like model, with parameters **A_0=1.96±0.20, A_1=0.62±0.41 and A_2=-0.53±0.20** and then a steeper spectrum component that becomes apparent below 1 GHz that is fit using a power-law with α=1.05±0.07 and A=80.2±1.5.
A1774
2MASX J13410515+3959456, z=0.1715. The SED of this source is consistent with a single power-law fit with parameters of α=0.61±0.03 and A=104.9±5.0, that persists to high frequency. Note that the FIRST (White *et al.* 1997) datum-point was removed from this fit as it appears to have resolved out some emission. The source appears one-sided in FIRST but the core is not isolated and the lack of higher-resolution data therefore means that a separate core component cannot be fit. The intermediate spectral index combined with the resolved morphology suggests that an active core is likely to be present in this system, which may be distinguishable with higher resolution observations.
A1795
CGCG 162-010, z=0.0632. Extended source with several observations of high enough resolution to create a separate SED for the isolated core only (see Laurent-Muehleisen *et al.* 1997; Lin & Mohr 2009; Liuzzo *et al.* 2009). This core spectrum is flat to high frequency, and fit using a power-law with α=0.65±0.06 and A=120.2±14.2. The SED of the more extended emission appears to exhibit spectral curvature to high frequency, hence to account for this we allow an exponential rollover to the steep power-law, of the form:

$$S = A\nu^{-\alpha}(1 - Be^{-\frac{\nu_0}{\nu}}) \quad \text{(A3)}$$

(Hogan *et al.* 2015a). The best fit returns parameters **A=1262.8, α=0.86, B=1.07 and ν_0=7.51 for the unknown parameters in this model.**
A1885
2MASX J14134379+4339450, z=0.090. The SED is core dominated with a hint of variability seen from historical C-band observations (Laurent-Muehleisen *et al.* 1997; Gregory & Condon 1991). Additionally, the WENSS (Rengelink *et al.* 1997) detection alongside the VLSS (Cohen *et al.* 2007) non-detection shows that the spectrum must peak in the GHz range. The SED can be fit with a GPS model, returning parameters of 1.66±0.03, 0.24±0.04 and -0.33±0.03.
A2052
UGC 09799/3C 317, z=0.0355. A separate core only SED can be created for the resolved isolated core. This can be fit with a GPS model (returning parameters; 2.54±0.02, 0.10±0.02 and -0.24±0.01). Accounting for this core contribution, fit a power-law (with α=1.20±0.08 and A=6404.5±1142.8) to the lower frequency emission. Note that there are a number of very low frequency (less than 50MHz) data-points that are flatter than this steep spectrum would imply. These are possibly affected by free-free absorption and hence were excised from the power-law fit.
A2055
2MASX J15184574+0613554, z=0.1019. High resolution data reveals an underlying core component with a GPS-like spectrum. Note that the CARMA datum is tagged as potentially unreliable and indeed appears inconsistent and has therefore been excluded from the fit. A GPS fit to the

core-only SED returns parameters of 1.28±0.04, 1.13±0.02 and -0.57±0.01. The integrated SED is increasingly dominated by a power-law component at frequencies less than 1 GHz. Fit this separately, accounting for the expected core contribution, to recover a power-law fit with α=0.70±0.04 and A=519.2±122.7.

A2270

2MASX J17272346+5510538, z=0.2473. Source appears highly variable. There is a limit only in the VLSS-redux catalogue (Lane *et al.* 2014) but an overlay of the map shows there to be a 3σ map detection at the optical position of the BCG. Along with other low frequency detections from 7C (Hales *et al.* 2007) and WENSS (Rengelink *et al.* 1997), this hints at there being a low-powered low frequency power-law component within this source. The data are widely spaced in observation date, making separate fits by epoch for the GPS component unfeasible. Fitting a GPS to fit to all the available data at higher frequencies than L-band, recovers an average GPS with parameters **A_0=2.11±0.06, A_1=0.56±0.06 and A_2=-0.31±0.04**. Account for the contribution of this to the lower frequency data and find a resultant power-law component with α=0.94±0.07 and A=28.0±0.7

A2390

ABELL 2390:[YEA96] 101084, z=0.2328. The spectrum appears to have a split power-law like shape below 10 GHz although the higher frequency observations show that the active component curves. Hence the SED is best fit using a combination of a GPS component (that returns parameters; 2.28±0.03, 0.26±0.04 and -0.42±0.05) and then a power-law component with α=1.34±0.25 and A=121.5±60.6. **Smail *et al.* (2002) claim a 6.7mJy SCUBA detection at 330 GHz for this source. This suggests that there may be additional intermittent activity at these higher frequencies or alternatively there may be a dust component coming in (although non-detection (<60mJy) at 660 GHz opposes this). Note that we do not include this claimed detection on our SED, including only our more contemporaneous upper-limit at 330 GHz.**

A2415

2MASX J22053865-0535330, z=0.0573. The SED has a flat index from around 1 GHz up to high frequency although a subtle drop-off means that this is best fit with a broad-peaked GPS model (returned parameters: 2.09±0.08, 0.26±0.02 and -0.29±0.01) in addition to a steep power-law component at lower frequencies with α=1.31±0.02 and A=193.2±9.4.

A2597

PKS 2322-12, z=0.0830. Source appears very flat to higher frequencies. Archival VLA observations at C, X and U-bands from the NRAO Image Archive allow isolated core measurements which in conjunction with higher frequency data suggest a broad GPS-like core that is well fit with parameters **A_0=1.92±0.05, A_1=0.27±0.09 and A_2=-0.30±0.04**, although there may be further flattening to yet higher frequencies as suggested by SCUBA observations (Zemcov *et al.* 2007; Knudsen *et al.* 2008). Lower frequency data are fit with a power-law of α=1.18±0.06 and A=2336.4±13.4, where the data below 100 MHz have been excluded as here the spectrum flattens, possibly due to free-free affected. Note that a simple extrapolation of this power-law in conjunction with the GPS core gives a wholly inaccurate integrated spectrum and hence the older, extended component must roll-off at some frequency. This has been simulated here by subtracting the GPS from the simple power-law to give the presented curved spectrum.

A2627

This cluster has two bright galaxies in close proximity, both of which are radio-sources. The more dominant source - A2627(a) / B2 2334+23 'the BCG' - is at position 23:36:42.12 23:55:29.0 and z=0.126. The other galaxy - A2627(b) / 2MASX J23364245+2354442 is at position 23:36:42.47 23:54:44.6 and has a redshift given in NED as z=0.122. VLA C-band data (H15a) separates the sources and overlaying other maps onto this we see that at NVSS (**1.4 GHz, Condon *et al.* 1998)** and lower frequencies the sources are confused. They are similarly confused in our AMI maps. The BCG can be isolated in the CARMA map and a VLA-A array image from the NRAO Image Archive. These show it to be flat spectum. Along with the GISMO data, fit a flat spectrum power-law to this (α=0.37±0.06 and A=109.0±22.9). Morphologically, A2627(a) is core dominated although it does show some wispy emission that is likely to contribute at lower frequencies. A2627(b) is fainter (by roughly a factor of 4 at C-band) but appears to be steep spectrum and is likely to become increasingly dominant at lower frequency. Fit the integrated emission (accounting for the flat component) with a power-law of α=0.65±0.06 and A=499.8±6.4 noting that this is highly confused. We currently do not have sufficient coverage to fully deblend the sources.

A3581

IC 4374, z=0.0218. Flat spectrum core dominated system with hints of variation in repeat observations around C- and X-bands. Unresolved at VLA-A in a map from the NRAO Image Archive but the source is resolved on milli-arcsecond scales with the VLBA (Hogan *et al.* 2015c, in prep.). This small-scale resolved emission is linked to ongoing activity and the **integrated flux recovered** with the VLBA is consistent with lower resolution fluxes showing that source is core-only. Fit a power-law to the integrated SED (returning a fit of α=0.49±0.04 and A=758.2±6.9) and then highlight the VLBA peaks on the SED.

A496

MCG -02-12-039, z=0.0328. This source has a GPS-like core with a steeper power-law component to low frequency. The core is fit with the GPS-like model with parameters **A_0=1.45±0.02, A_1=0.60±0.02 and A_2=-0.43±0.03** and then accounting for this component, the remaining extended emission is fit with a power-law of α=1.71±0.03 and A=99.8±6.4.

A646

2MASX J08220955+4705529, z=0.1268. The SED of this source can be fit using a GPS model for the core component, which returns parameters 1.89±0.02, 0.14±0.01 and -0.25±0.08 and a power-law component of α=1.54±0.09 and A=13.5±0.3 to account for the lower frequency, extended emission. Note that the combination of these two components at 1.4 GHz over-estimates the NVSS flux (Condon *et al.* 1998) which may be attributable either to variation of the core component or perhaps indicating that this source should in reality have a more sharply peaked profile.

AS780

2MASX J14592875-1810453, z=0.2344. This **object** has previously **been** identified as a flat spectrum source (e.g. Healey *et al.* 2007). The GHz range flat spectrum falls off above about 20 GHz. The source is undetected in VLSS (Cohen *et al.* 2007), which suggests that the spectrum must turnover around 1 GHz. The SED is fit with a GPS model, that returns parameters 2.16±0.02, 0.34±0.02 and -0.35±0.01. Note that the source is mildly confused in the WISH map **(De Breuck *et al.* 2002)**. The flux used here is deblended BCG emission however there could still be wrongfully attributed flux contributing to this 352 MHz measurement. Equally, this 352 MHz point lying above the curve could be indicative of a steeper spectrum component (which would push the GPS peak to higher frequency). Future low frequency observations will determine this.

E1821+644

HB89 1821+643, z=0.2970. This source is one of the few radiatively efficient AGN known to reside within a cool core cluster (see e.g. Russell *et al.* 2010, and references therein). Nevertheless, the radio-properties appear to be consistent with its more inefficent brethren. Multiple high resolution VLA observations from the NRAO Image Archive allow the core to be isolated at multiple frequencies which are consistent with the spectral flattening seen above about 10 GHz. The source shows significant variation. Fit the core-only measurements with a GPS-like model, returning parameters of 0.83±0.10, 0.40±0.06 and -0.19±0.03. This suggests a broad, flat profiled core. Independently fit a steep power-law to the low frequency data, returning a fit with α=1.06±0.13 and A=94.6±3.6.

Hydra-A

This source is associated with the bright radio source 3C 218, z=0.0549. This source is very well studied (e.g. McNamara *et al.* 2000; Hamer *et al.* 2014, and references therein). VLBA observations at multiple frequencies (e.g. Taylor 1996; Araya *et al.* 2010) allow the SED of the core only to be independently fit with a GPS model (returning parameters: 2.01±0.05, 0.95±0.06 and -0.59±0.06). The integrated SED is dominated by flux from the extended emission and remains persistent to frequencies higher than 100 GHz. Accounting for the minimal core contribution, fit the SED using a power-law with α=1.00±0.02 and A=47214.3±43.0.

MACS0242-21

PKS 0240-217, z=0.314. This source appears to be a CSS or low-peaking GPS, that can be fit using a GPS model with parameters of $\mathbf{A_0}$**=3.14±0.02,** $\mathbf{A_1}$**=-0.14±0.02 and** $\mathbf{A_2}$**=-0.30±0.02**. VLBA observations of the source at S- and X-band (Beasley *et al.* 2002) show that it is 'wispy' on parsec scales, with the integrated flux consistent with the unresolved emission at VLA resolutions. That the source has a low spectral peak, alongside it being very structured on parsec scales, is consistent with this source being in a late-stage of core activity.

MACS1931-26

PMN J1931-2635, z=0.3520. There are two radio-sources in close proximity within the cluster core; the BCG at 19:31:49.67 -26:34:33.4 and a Wide-Angled Tail (WAT) source, PMN 1931-2635, at 19:31:50.0 -26:35:16.4. These sources are confused in many radio maps of the region. The BCG core is isolated in ATCA-6km observations at 5.5 and 9.0 GHz along with CARMA and GISMO at higher frequencies. The SED of only these points is well fit with a GPS model, returning parameters 0.95±0.04, 0.42±0.03 and -0.21±0.01. The sources are confused in lower resolution observations. The sources cannot therefore be fully distinguished, however by fitting to the flux peaks coincident with the optical positions it appears as if PMN 1931-2635 has a steeper spectrum (as would be expected for a lobe-dominated WAT). Further confounding the picture, high resolution VLA-A observations at L-band by Ehlert *et al.* (2011) show that the BCG is surrounded by an amorphous halo (see also Mittal *et al.* 2009) that is likely to be very steep spectrum. This structure is most likely confused emission from previous activity cycles of the BCG (Hogan *et al.* 2015a). The integrated emission of this amorphous halo component does not account for all of the flux in the confused observations. However, such high resolution observations at other frequencies to fully detangle this amorphous halo emission are not available currently. Shown on the SED are the core only observations along with highlighted confused, amorphous halo and WAT data points.

RXJ0132-08

PKS 0130-083, z=0.1489. This source appears to be either a low-peaking GPS or a CSS. The source does not appear above the 5σ cut-off of the VLSS catalogue (Cohen *et al.* 2007) but overlaying the VLSS map, the source is present at the optical position as a 3σ detection. The central engine is resolved in VLBI maps (Bourda *et al.* 2010, 2011; Petrov 2011, []). Fit a GPS model to the integrated emission (that returns parameters; 2.55±0.04, -0.24±0.03 and -0.11±0.03) and show the VLBI peaks on the SED (although note that these are not included in the fit).

RXJ0352+19

2MASX J03525901+1940595, z=0.109. The SED is relatively poorly sampled, consisting of only four detections and limits from the pointed GISMO observation (at 150 GHz) and the VLSS (Cohen *et al.* 2007). A single power-law fit returns α=0.41±0.18 and A=20.4±5.8, which is consistent with the limits and suggests a flat spectrum source. However, there could be a small GPS-like component with a tail but available data are not sufficient to confirm nor deny this, hence the power-law is perhaps the most robust fit possible with current data.

RXJ0439+05

2MASX J04390223+0520443, z=0.208. The SED can be well fit with a strong GPS component, that returns parameters 1.42±0.03, 1.67±0.02 and -0.72±0.01 and then a steep spectrum tail to lower frequency (less than 1 GHz) with α=1.10±0.04 and A=60.2±5.5.

RXJ0747-19

PKS 0745-191, z=0.1028. The SED potentially flattens below around 200 MHz but other than that presents as a steady power-law out to higher than 150 GHz, with α=1.26±0.07 and A=3064.7±23.4.

RXJ1347-11

GALEX J134730.7-114509, z=0.450. The BCG is surrounded by a confirmed 500kpc radio mini-halo (see Gitti *et al.* 2007). Using high resolution VLA observations from the NRAO Image Archive, an SED of only the BCG is created. This suggests an active AGN, whose SED is well fit with the GPS model with parameters of $\mathbf{A_0}$**=1.35±0.05,**

A_1=0.30±0.01 and A_2=-0.35±0.01. The mini-halo emission has a steep spectrum with α=1.20±0.04 and A=47.2±4.1. The similarity of the SED of this source to other observed spectra in systems without observed mini-halos, but with smaller amorphous haloes lends evidence to the belief that the seed populations for true mini-haloes are built from repeated AGN activity in the BCG (Hogan *et al.* 2015a).

RXJ1350+09

2MASX J13502209+0940109, z=0.1325. This source appears to be highly variable, and has previously been identified as a BL-LAC (e.g. Massaro *et al.* 2009; Richards *et al.* 2011). A non-detection in the VLSS (Cohen *et al.* 2007) shows that this source has no steep component at low frequencies and hence the SED appears to be GPS-like. Fit the SED with a GPS model, which returns a sharp peaked spectrum with parameters **A_0=2.42±0.04, A_1=0.70±0.03 and A_2=-0.65±0.03**.

RXJ1504-02

LCRS B150131.5-023636, z=0.2171. This cluster contains a confirmed radio mini-halo (Giacintucci *et al.* 2011), 140kpc in extent. This mini-halo manifests itself as a steep spectrum tail in the SED to low frequencies (below about 1 GHz). There appears to be an active core within the central BCG that gives rise to a GPS-like component in the integrated SED, that can be fit using the GPS model with parameters **A_0=1.67±0.01, A_1=-0.09±0.01 and A_2=-0.16±0.04**. The mini-halo emission can be isolated from that of the AGN at L-band (White *et al.* 1997) and agrees well with lower frequency data (see SED), giving a power-law fit to this lower frequency component with α=1.19±0.05 and A=31.4±3.9.

RXJ1558-14

PKS 1555-140, z=0.0970. This is an actively evolving system with good historical coverage. See section 5.2 for a more detailed description of this system. Here we perform an average GPS model fit of the core over the previous 40 years, recovering parameters of 2.69±0.04, 0.31±0.10 and -0.45±0.06 and then fit a power-law for the steep spectrum tail which has α=1.30±0.20 and A=71.6±4.0.

RXJ1715+57

NGC6338, z=0.0282. Considering the archival C-band measurements (e.g. Gregory & Condon 1991) suggests that this source may show some long-term variability in here. Without the GISMO observation the SED would perhaps be interpreted as a GPS, however the 150 GHz detection shows that the spectrum remains flat up to high frequency. The GISMO flux could be interpreted as evidence of 'flickering' at high frequencies or variability. Either way, the SED is most reliably fit using a power-law with α=0.41±0.04 and A=53.1±3.1. This shows the source to be flat spectrum and is consistent with the non-detection in VLSS (Cohen *et al.* 2007).

RXJ1832+68

2MASX J18323551+6848059, z=0.205. The SED is dominated by steep spectrum emission to about 10 GHz that is fit using a power-law with α=0.92±0.03 and A=194.8±7.7. Above this frequency the spectrum appears to 'bump' outwards. VLBA observations (Hogan *et al.* 2015c) at C-band show that there is an active core component in here (see also Laurent-Muehleisen *et al.* 1997). By considering measurements of the core flux only, this active component can be well fit with a relatively high-peaking GPS component with returned parameters of 0.78±0.36, 1.31±0.53 and -0.56±0.20. When combined with the power-law this interpretation appears to well explain the integrated spectral shape.

RXJ2341+00

PKS 2338+000, z=0.2767. This is an unresolved radio source (at few-arcsecond resolution) whose SED is steeper at higher frequency yet is flattening at less than a few GHz. The 365 MHz flux from the TEXAS survey (Douglas *et al.* 1996) shows that the SED does turnover. Fit the SED with a low peaking GPS, with returned parameters of 2.62±0.01, -0.16±0.06 and -0.15±0.04. This source is a non-detection at the 5σ detection limit of the VLSS catalogue (Cohen *et al.* 2007), and the limit is consistent with the inferred turnover. Looking at the VLSS map overlaid onto an optical image of the region, we see that there is a faint (<3σ) detection at the correct position. This point was not included in the fit but is included on the SED to highlight that it is consistent with being a genuine detection.

Z235

2MASX J00435213+2424213, z=0.083. The SED of this source has a flat spectral index, that can be fit with a single power-law of α=0.45±0.06 and A=61.7±7.3. The returned index is consistent with the non-detection in VLSS (Cohen *et al.* 2007).

Z8193

B3 1715+425, z=0.1754. This source appears to contain a variable core component that is confirmed by VLBI measurements (Bourda *et al.* 2010, 2011, see also Hogan *et al.* 2015c, in prep). The SED is fit by a combination of a GPS model to account for the spectral flattening above about 1 GHz and a steep power-law tail to lower frequencies. Note that the source is below the detection threshold of the VLSS catalogue (Cohen *et al.* 2007) but appears as a ≈3σ detection at the correct position in the map overlay. The flux is therefore retrived using the AIPS task IMFIT from a VLSS cut-out. The returned parameters for the GPS component are 1.82±0.01, 0.26±0.01 and -0.26±0.01. Accounting for the core contribution, a power law with α=0.82±0.04 and A=89.2±5.7 is fitted to the low frequency tail.

Z8276

2MASX J17441450+3259292, z=0.075. There is a distinct split in the spectral index of the SED at approximately 1 GHz. There also appears to be large amplitude variability at higher frequencies. Fit the steeper component using a power-law with α=1.26±0.03 and A=80.0±6.0 and then fit the GPS model to the core only measurements, which returns GPS-model parameters of 1.57±0.50, 0.52±0.76 and -0.30±0.26.

This paper has been typeset from a TEX/ LATEX file prepared by the author.

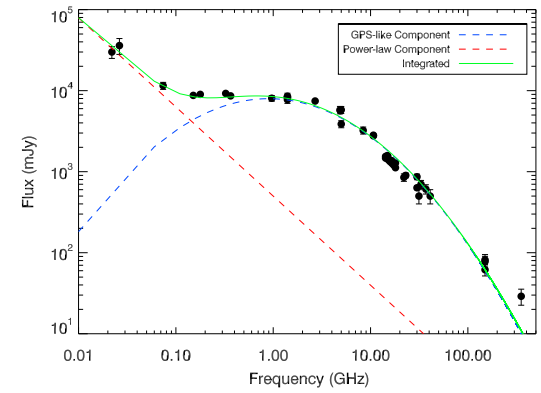

(a) *4C+55.16*

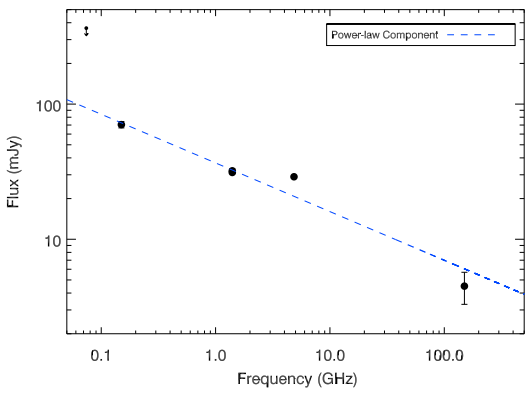

(b) *A1084*

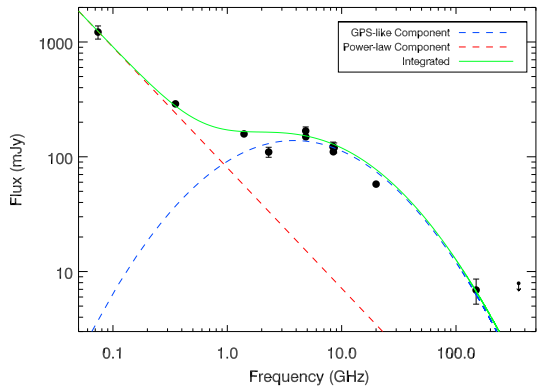

(c) *A1348*

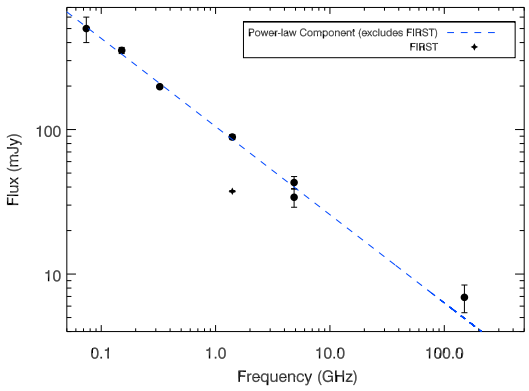

(d) *A1774*

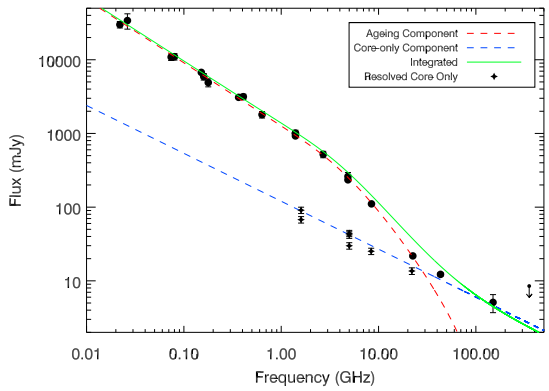

(e) *A1795*

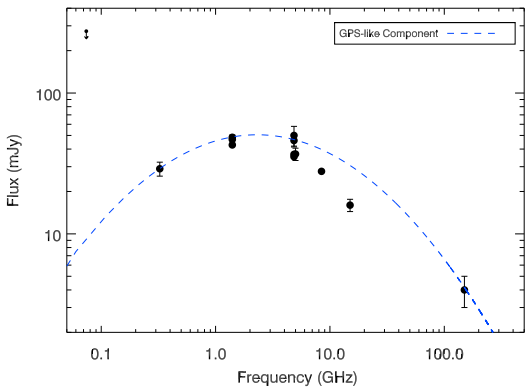

(f) *A1885*

Figure A1. SEDs for sources withing our sample. Typically, data-points represent the spatially-integrated flux density at the given frequency. In many cases this is dominated by either the core, or the extended emission, as indicated by the fits. Core only data-points have been highlighted for instances where a separate SED was fitted for cores that could be morphologically isolated, to differentiate these from instances where the integrated flux shows clear variability. Likewise, other 'special' cases have been indicated on the plots.

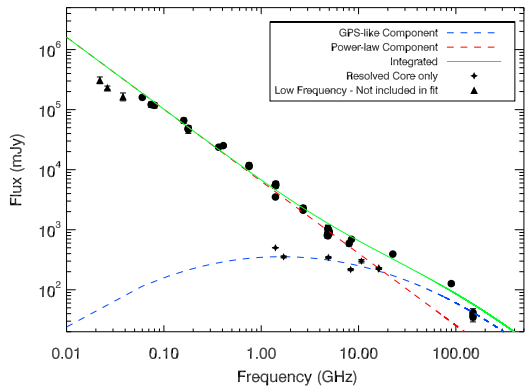

(a) *A2052*

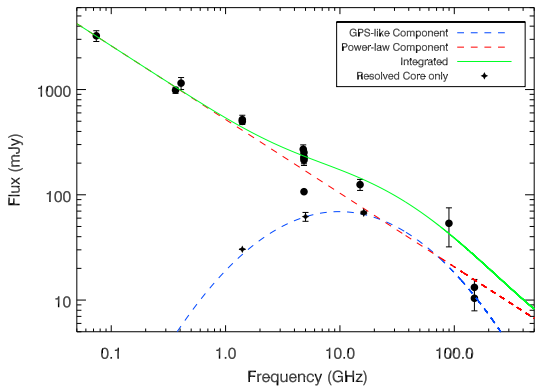

(b) *A2055*

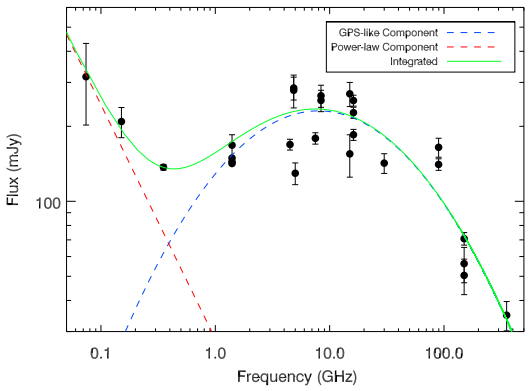

(c) *A2270*

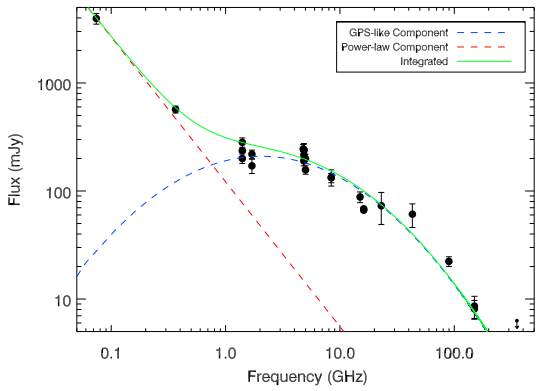

(d) *A2390*

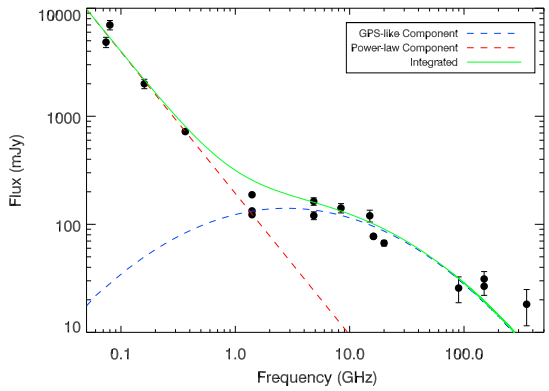

(e) *A2415*

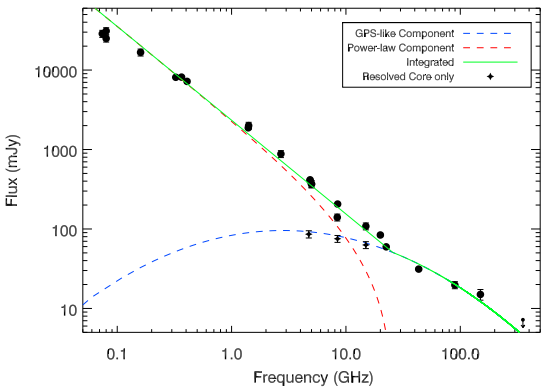

(f) *A2597*

Figure A2. SEDs, continuation of Fig. A1

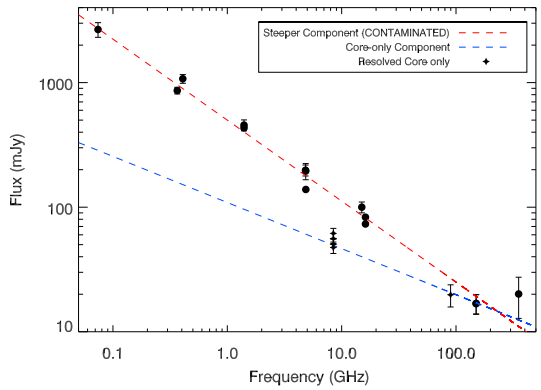

(a) *A2627*

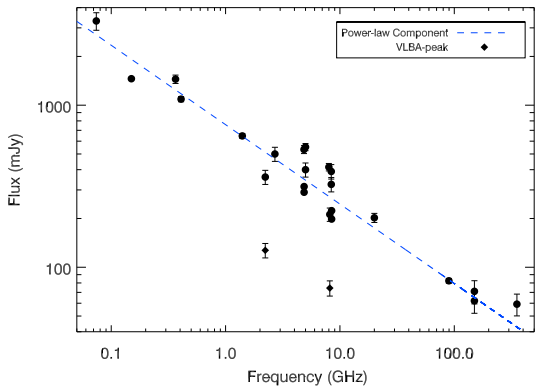

(b) *A3581*

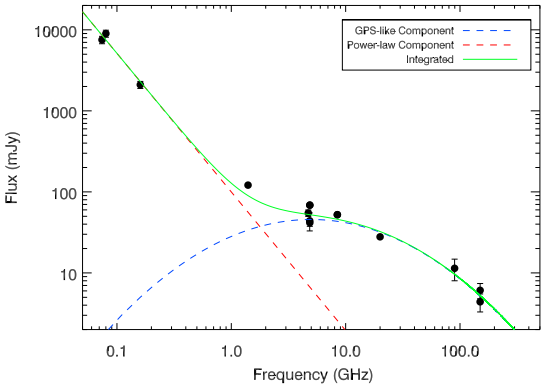

(c) *A496*

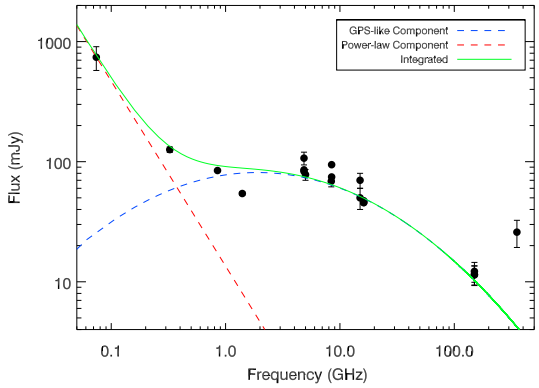

(d) *A646*

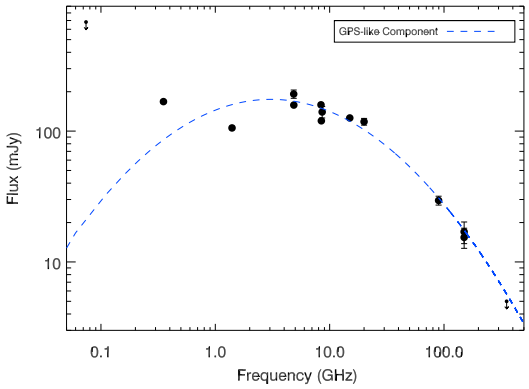

(e) *AS780*

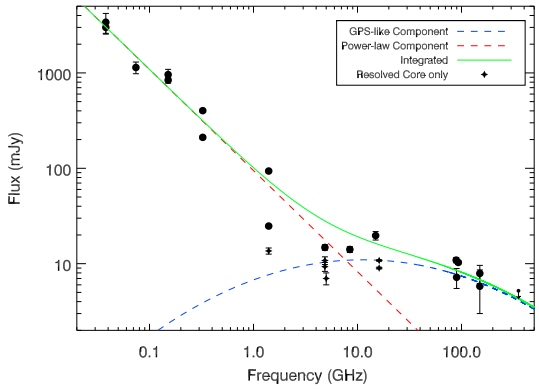

(f) *E1821+644*

Figure A3. SEDs, continuation of Fig. A1

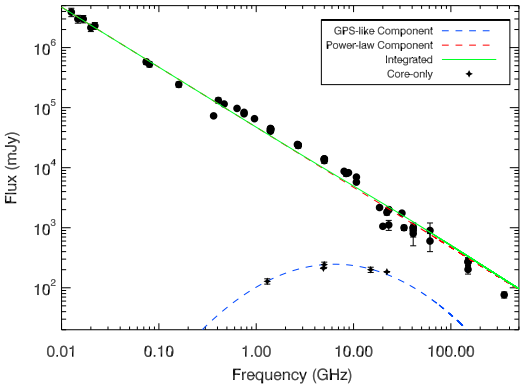

(a) *Hydra-a*

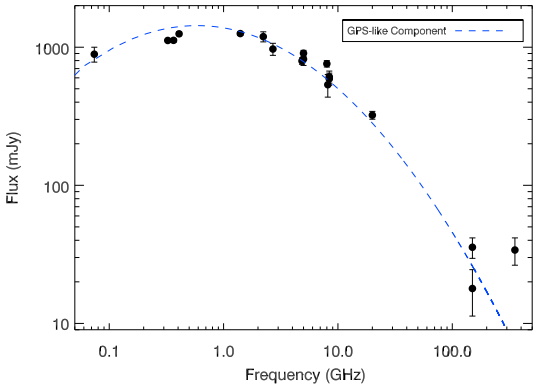

(b) *MACS0242-21*

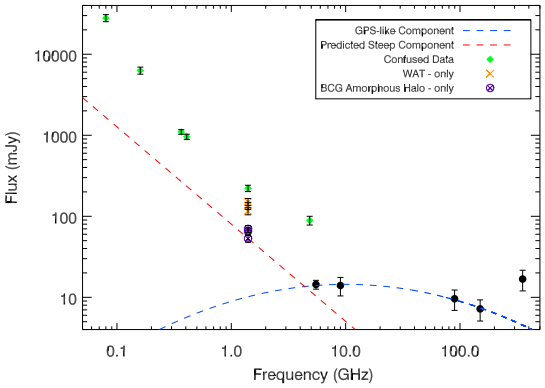

(c) *MACS1931-26*

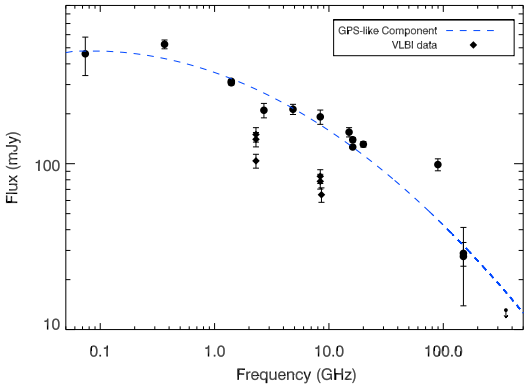

(d) *RXJ0132.6-0804*

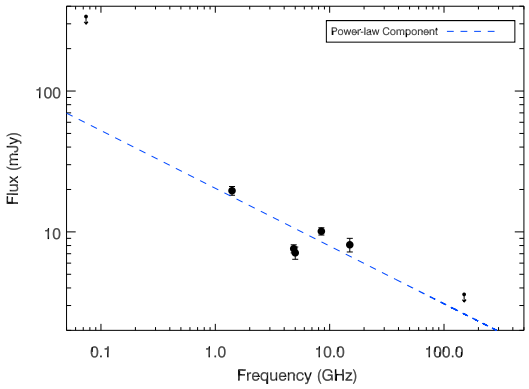

(e) *RXJ0352.9+1941*

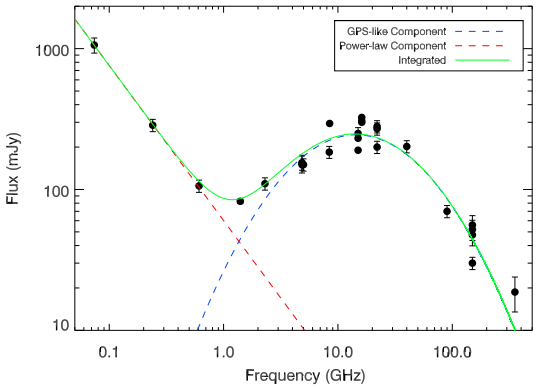

(f) *RXJ0439.0+0520*

Figure A4. SEDs, continuation of Fig. A1

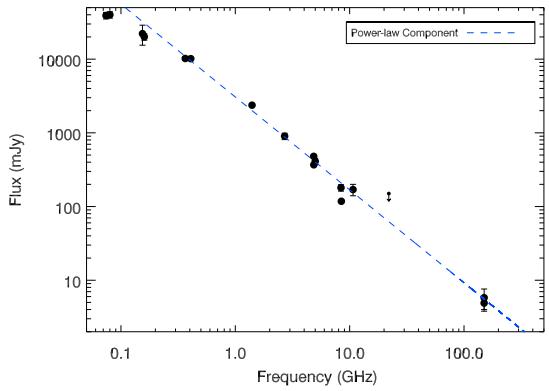

(a) *RXJ0747.5-1917*

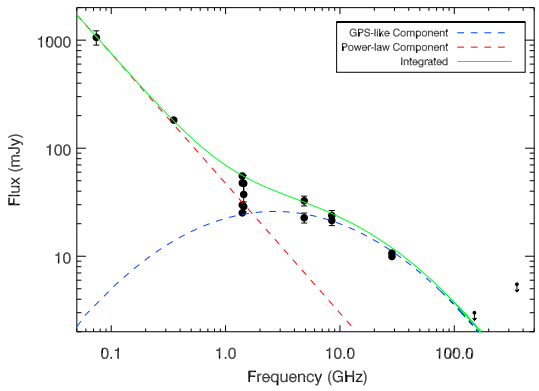

(b) *RXJ1347.5-1145*

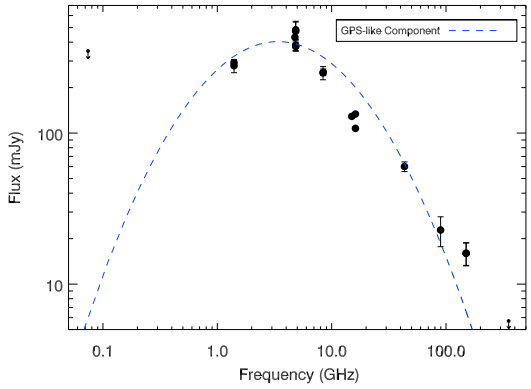

(c) *RXJ1350.3+0940*

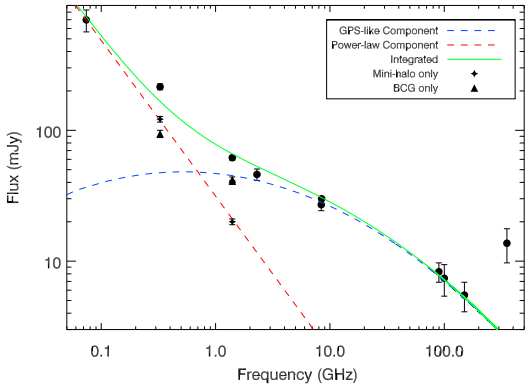

(d) *RXJ1504.1-0248*

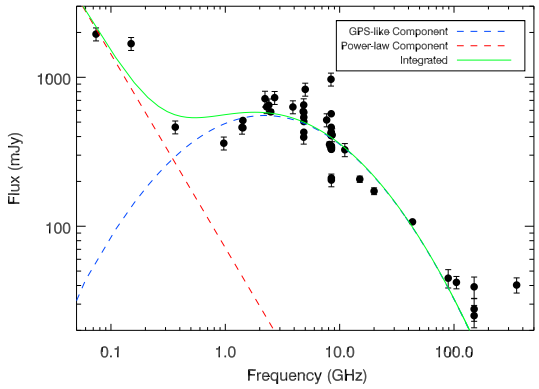

(e) *RXJ1558.4-1410*

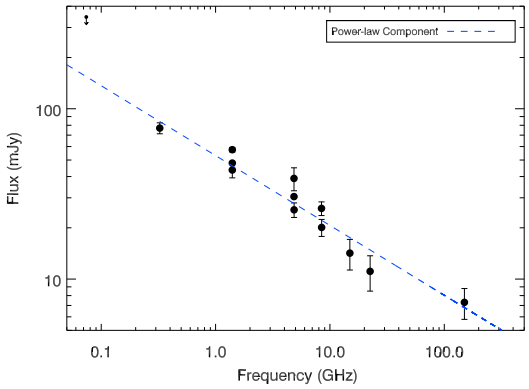

(f) *RXJ1715.3+5725 (NGC6338)*

Figure A5. SEDs, continuation of Fig. A1

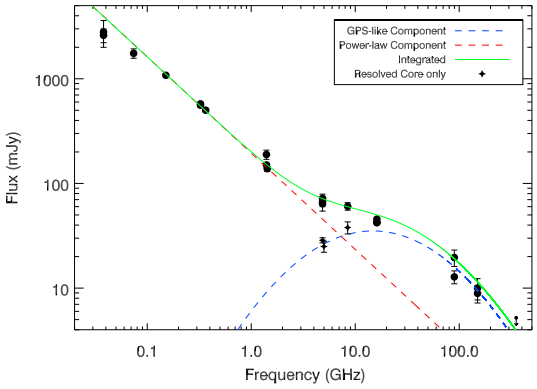

(a) *RXJ1832.5+6848*

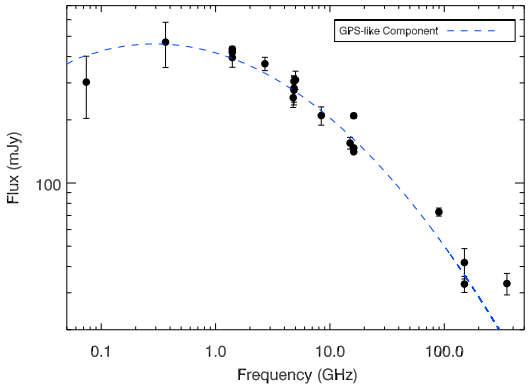

(b) *RXJ2341.1+0018*

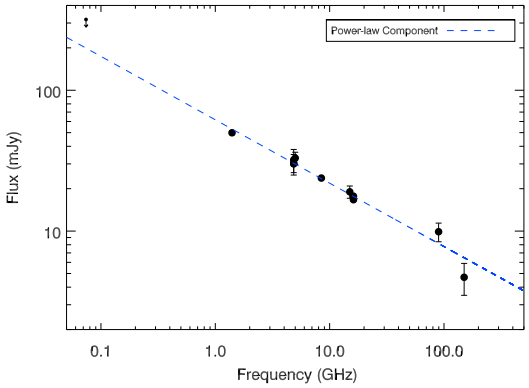

(c) *Z235*

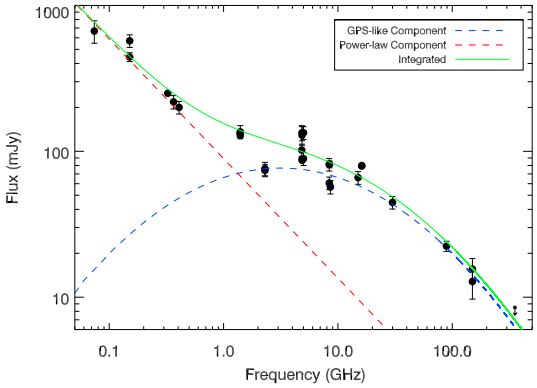

(d) *Z8193*

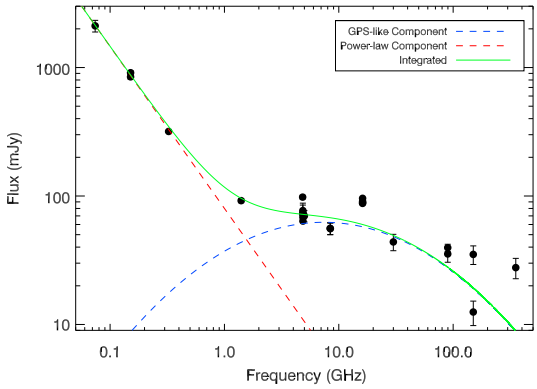

(e) *Z8276*

Figure A6. SEDs, continuation of Fig. A1